Electronic Supplementary Information for

# Trinuclear Copper(I) Furanyl *ortho*-Diphosphine Halide Clusters: Structure, Photophysical and Photocatalytic Hydrogen Production Properties

Xiang Chen[a], Li Liu[a,*], Xin-Xin Zhong[a,*], Heng-Jiang Cong[b,*], Feng-Yan Li[c,*], Fa-Bao Li[a,*], Yi Zhao[d]

[a] *College of Chemistry and Chemical Engineering, Ministry of Education Key Laboratory for the Synthesis and Application of Organic Functional Molecules, Hubei University, Wuhan 430062, P. R. China. E-mail: liulihubei@hubu.edu.cn, xxzhong@hubu.edu.cn, lfb0615@hubu.edu.cn*

[b] *College of Chemistry & Molecular Sciences, Wuhan University, Wuhan 430072, Hubei Province, P. R. China. E-mail: conghj@whu.edu.cn*

[c] *Key Laboratory of Polyoxometalates Science of Ministry of Education, College of Chemistry, Northeast Normal University, Changchun 130024, P. R. China. E-mail: lify525@nenu.edu.cn*

[d] *Department of Chemistry, State Key Laboratory of Physical Chemistry of Solid Surfaces, Xiamen University, Xiamen 361005, P. R. China.*

Electronic supplementary information (ESI) available: DETAILS. CCDC2266626-2266628.

## Contents

## 3. Photophysical Properties



## 4. Theoretical calculation

**Table S4**. Computed excitation transitions for complex **3** in $CH_2Cl_2$.

## 1. General information

*Materials.* All chemicals were purchased from commercial sources and used without being processed unless specified. The starting material in Scheme 1, 3,4-dibromofuran was synthesized according to the literature method.[1] Diethyl ether ($Et_2O$) were distilled under nitrogen in the presence of sodium chips with benzophenone as the indicator before use.

*Instrumentation*. $^{1}H$, $^{13}C$ and $^{31}P$ NMR spectra were recorded on a Varian 400 MHz NMR spectrometer using deuterated solvents as the lock and reference. Chemical shifts were referencesd to the solvent residual peak at 7.26 ppm for $^{1}H$ and 77.16 ppm for $^{13}C$ NMR spectra in $CDCl_3$, at 2.50 ppm for $^{1}H$ NMR in $d_6$-DMSO, at 5.30 ppm for $^{1}H$ NMR in $CD_2Cl_2$, respectively. High resolution mass spectra (HRMS) were recorded on the Thermo Scientific Exactive Plus equipped with electrospray ionization source. The elemental composition was determined with SEM/EDS (Hitachi SU-800 FE-SEM). UV–vis absorption was recorded by a Hewlett-Packard 8453 spectrometer. Emission spectra and lifetimes of the complexes were measured using Edinburgh instrument FLS980 steady-state and time resolved fluorescence spectrometer (375 nm variable pulsed diode laser, repetition frequencies 1000 Hz, and optical pulse period 100 ns). Solid-state $\Phi_{PL}$ values were determined using a Hamamatsu system for absolute PL quantum yield measurements equipped with an integrating sphere with Spectralon inner surface coating. Thermogravimetric analysis (TGA) was performed on a thermal analysis instrument (Perkin-Elmer Diamond) under nitrogen atmosphere at a heating rate of 20 °C $min^{-1}$.

*X-ray crystallography.* Crystals of complexes **1**–**3** suitable for X-ray diffraction studies were grown by slow evaporation of their respective solutions in dichloromethane/*n*-hexane at room

temperature. Geometric and intensity data were collected using Cu Kα radiation (λ = 1.54184 Å) on a XtaLAB Synergy, Dualflex, HyPix area detector. The collected frames were processed with the software *SAINT*[2], and an absorption correction was applied (*SADABS*)[3] to the collected reflections. The structures were solved by direct methods (*SHELXTL*)[4] in conjunction with standard difference Fourier techniques and subsequently refined by full-matrix least-squares analyses on $F^2$. All non-hydrogen atoms were assigned with anisotropic displacement parameters.

*Theoretical calculations.* The structural parameters for complexes **1–3** were obtained from the crystal data which are listed in Tables 1 and 2. The corresponding ground-state ($S_0$) geometries were all optimized at theoretical level of B3LYP-D3(BJ)/6-311+G(d,p) (LANL2D2 for Cu and I atoms), where D3(BJ) was Grimme's D3 dispersion correction with Becke-Jonson damping. To calculate the adiabatic excitation energies, the optimized geometries of $S_1$ and $T_1$ are required, which were obtained at theoretical levels of TD-B3LYP-D3(BJ)/6-31+G(d) and UB3LYP-D3(BJ)/6-31+G(d) (LANL2D2 for Cu and I atoms), respectively. The absorption spectra based on the optimized $S_0$ geometries were obtained at the TD-B3LYP-D3(BJ)/6-311+G(d,p) (LANL2D2 for Cu and I atoms) level. In addition, the solvent effects were taken into account by the polarizable continuum model (PCM, solvent = dichloromethane) for the purpose of comparing with the experimental spectra. All the calculations were manipulated by the Gaussian 16 suite.[5] The compositions of the frontier molecular and natural transition orbitals at optimized $S_0$, $S_1$, $T_1$ and $T_2$ geometries of complexes **1–3** were calculated by the Multiwfn program.[6,7]

*Photocatalytic hydrogen production*

The photocatalytic hydrogen production test was performed in a sealed quartz flask. A 300 W xenon lamp (Beijing Perfectlight Technology Corp., China) was used as the light source with an AM 1.5 optical filter and the photocurrent density was 100 mW $cm^{-2}$. In a typical photocatalytic experiment, 50 mg of the prepared photocatalyst (complexes **1–3** in powder state) was suspended in 150 mL of a mixed solution containing triethanolamine (TEOA, 15%) and methanol (MeOH, 20%) as sacrificial reagents and DI water. Nitrogen was purged through the cell for 30 minutes to remove oxygen before the photocatalytic reaction. The blank experiments showed no appreciable hydrogen evolution in the absence of irradiation or a photocatalyst.

2. NMR and mass spectra

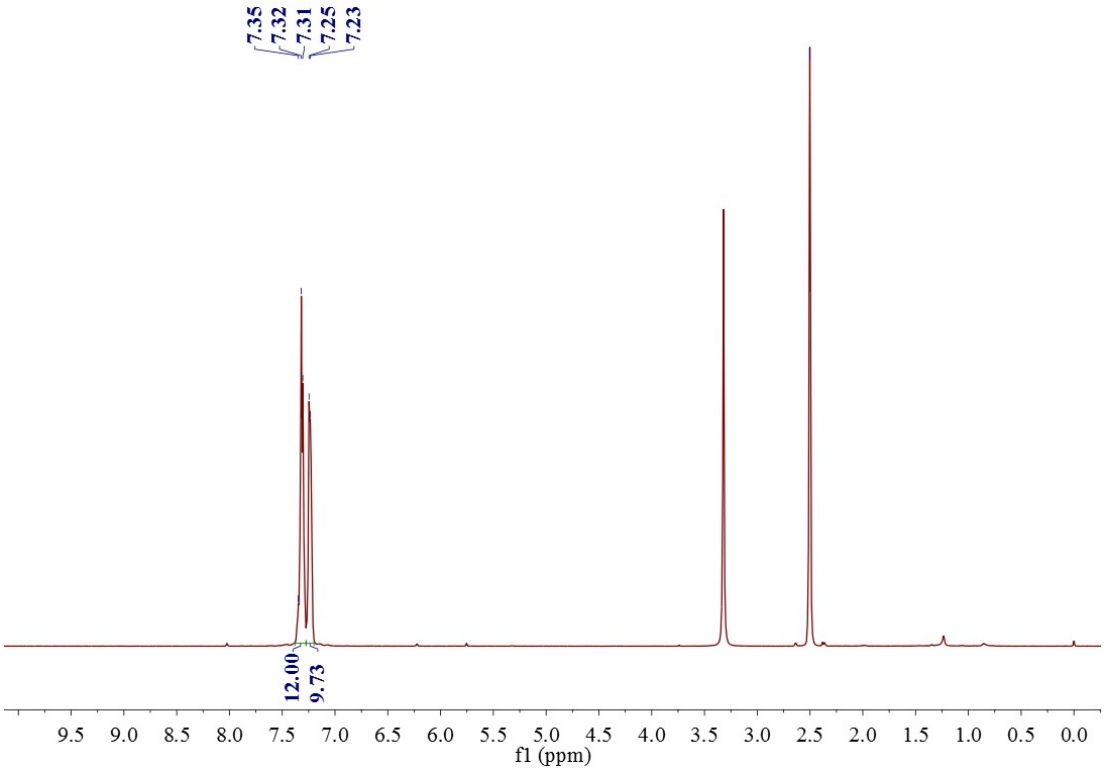


**Figure S1**. $^{1}$H NMR spectrum of **dppf** in $d_6$-DMSO ($\delta$ = 2.50, solvent residual peak; $\delta$ = 3.33, $H_2O$).

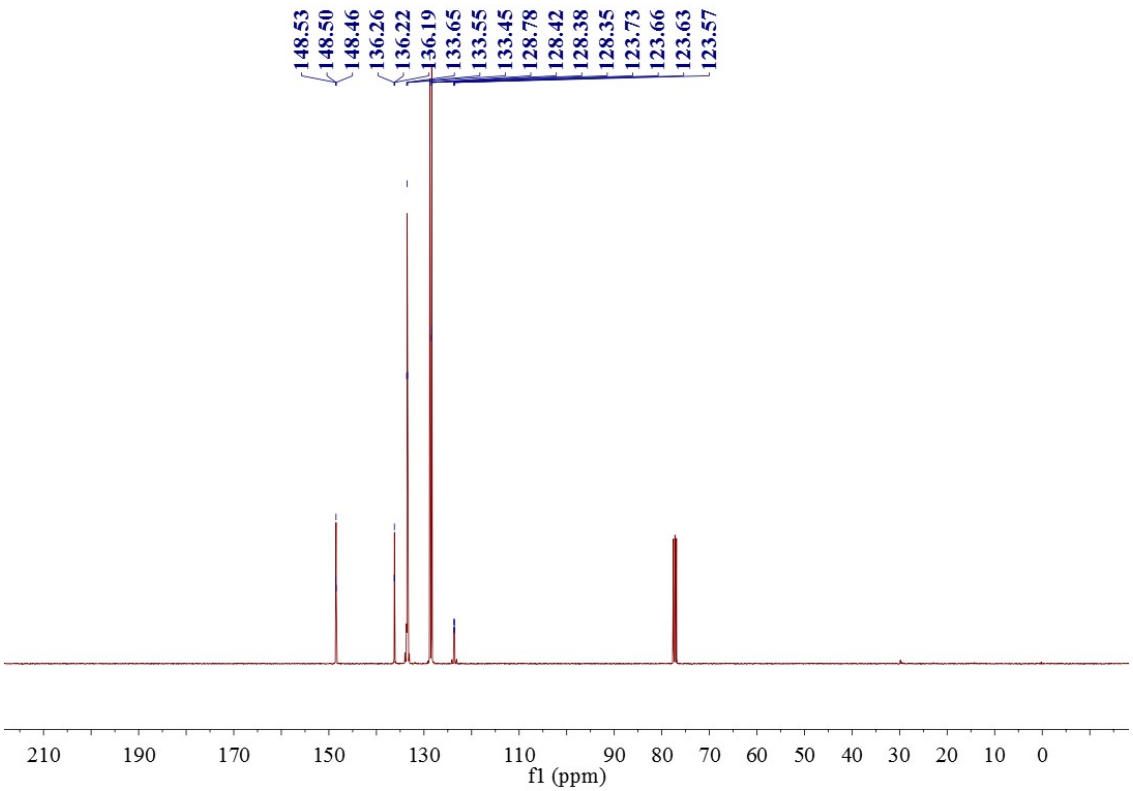


**Figure S2**. $^{13}$C NMR spectrum of **dppf** in $CDCl_3$.

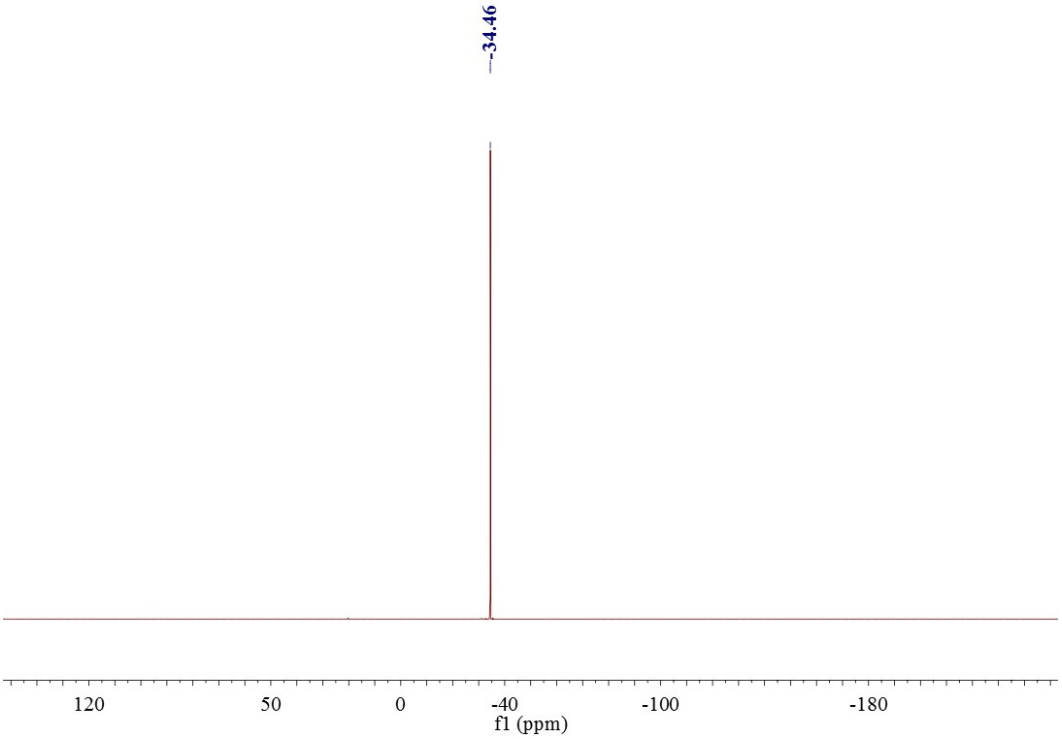


**Figure S3**. $^{31}P$ NMR spectrum of **dppf** in $CDCl_3$.

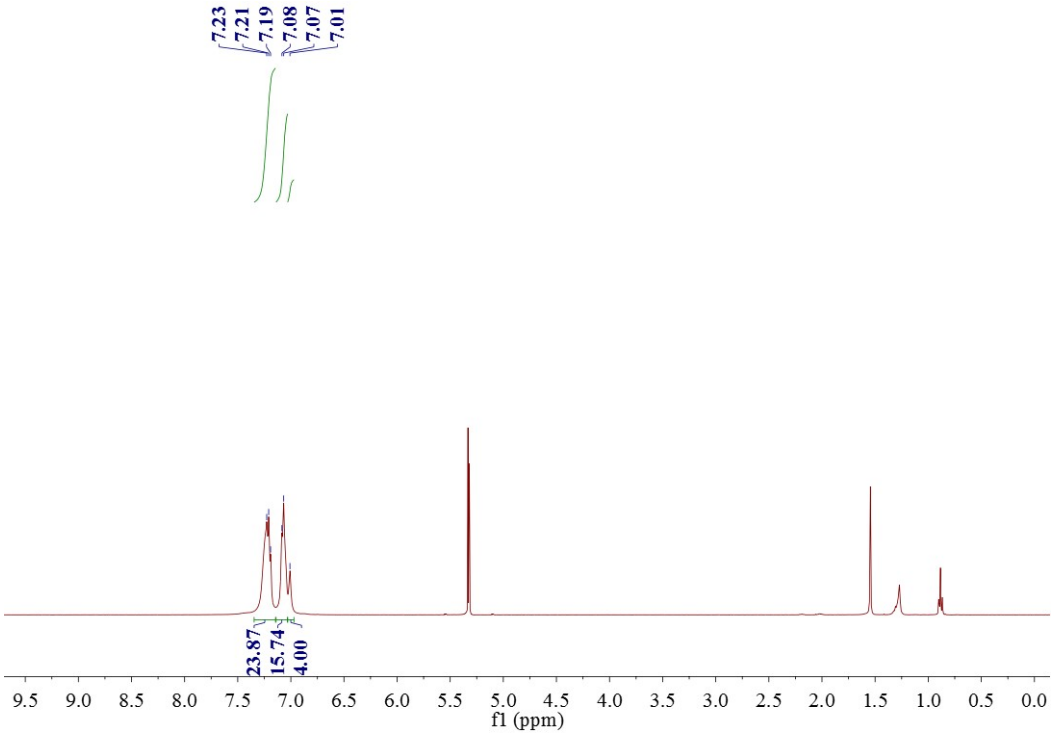


**Figure S4**. $^{1}H$ NMR spectrum of **1** in $CD_2Cl_2$ ($\delta$ = 5.30, solvent residual peak).

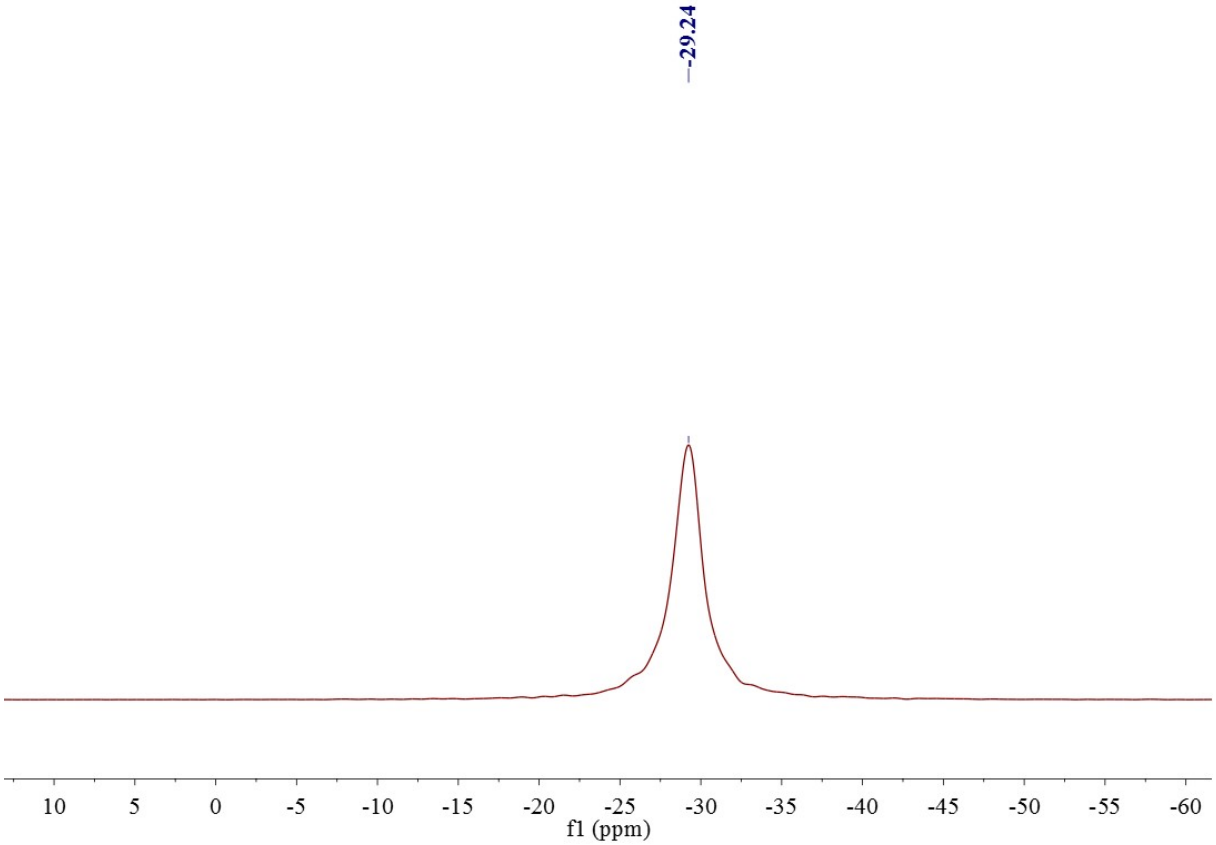


**Figure S5**. $^{31}P$ NMR spectrum of **1** in $CDCl_3$.

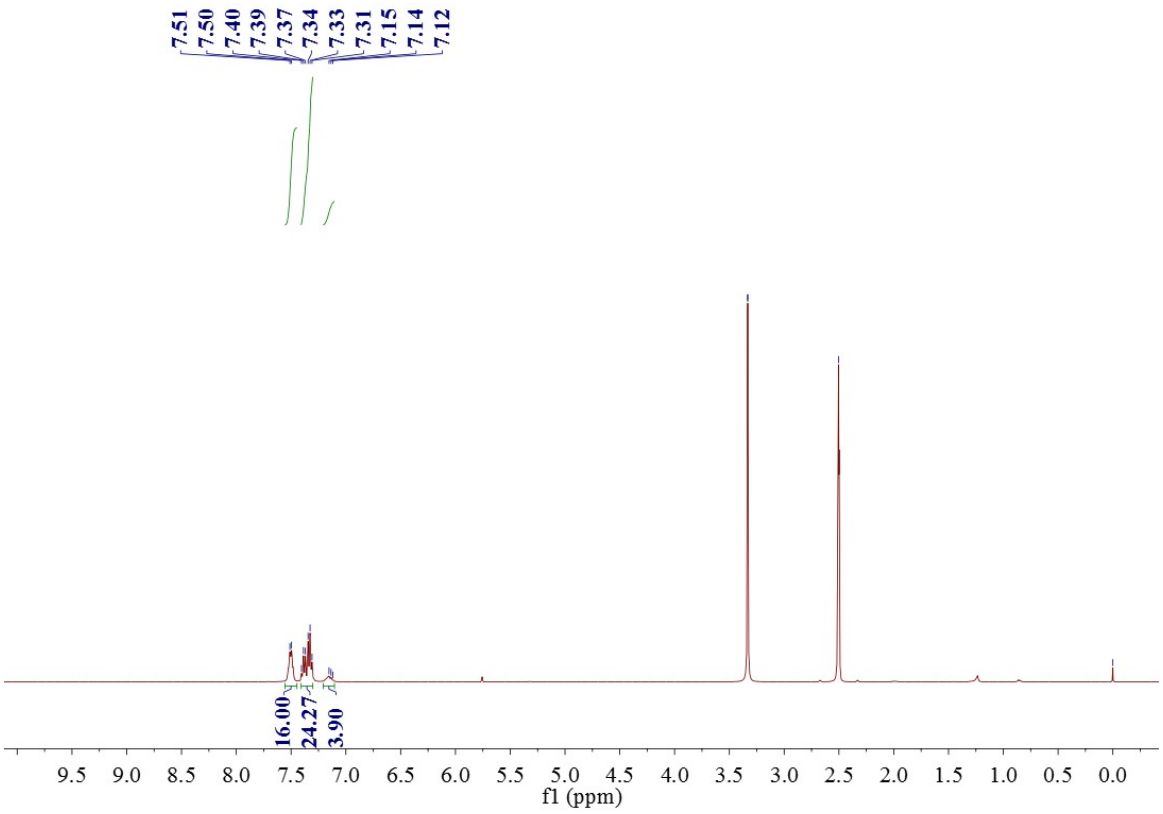


**Figure S6**. $^{1}H$ NMR spectrum of **2** in $d_6$-DMSO.

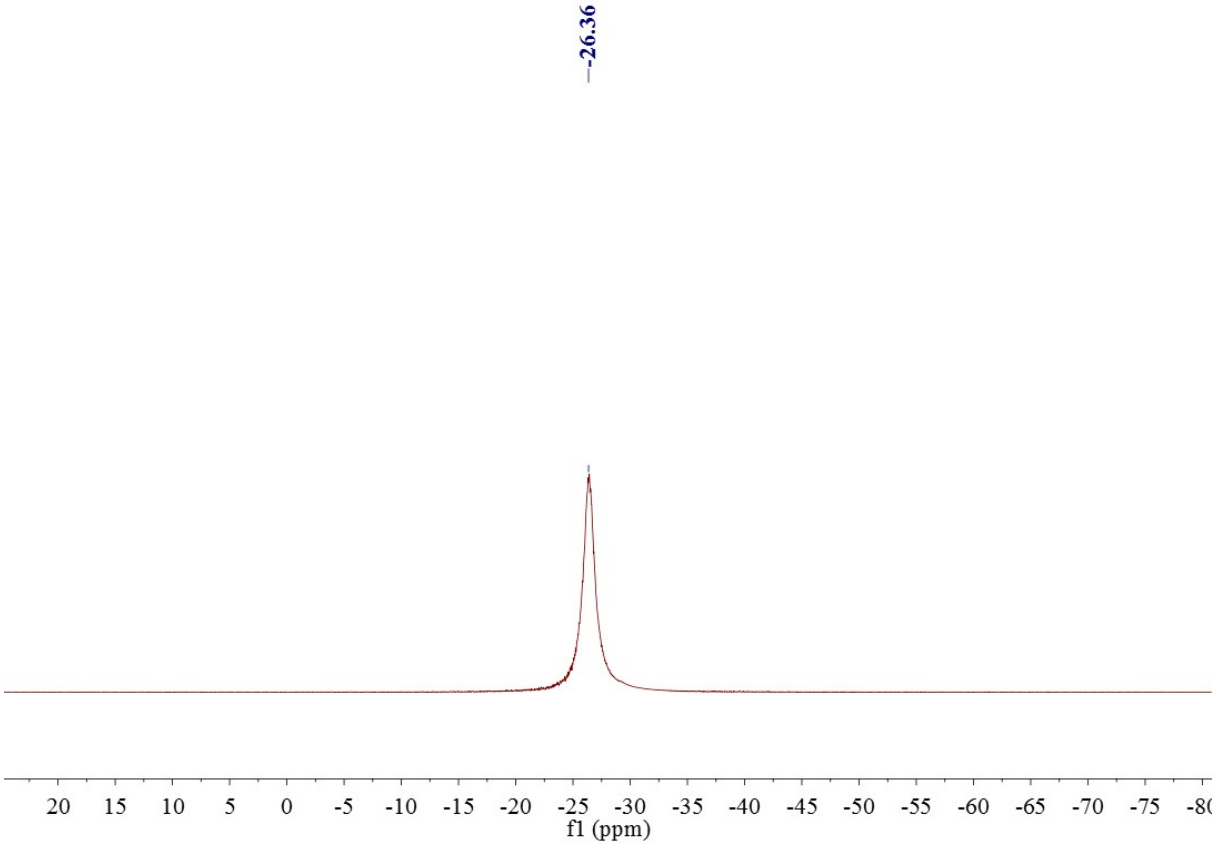


**Figure S7**. $^{31}P$ NMR spectrum of **2** in $CDCl_3$.

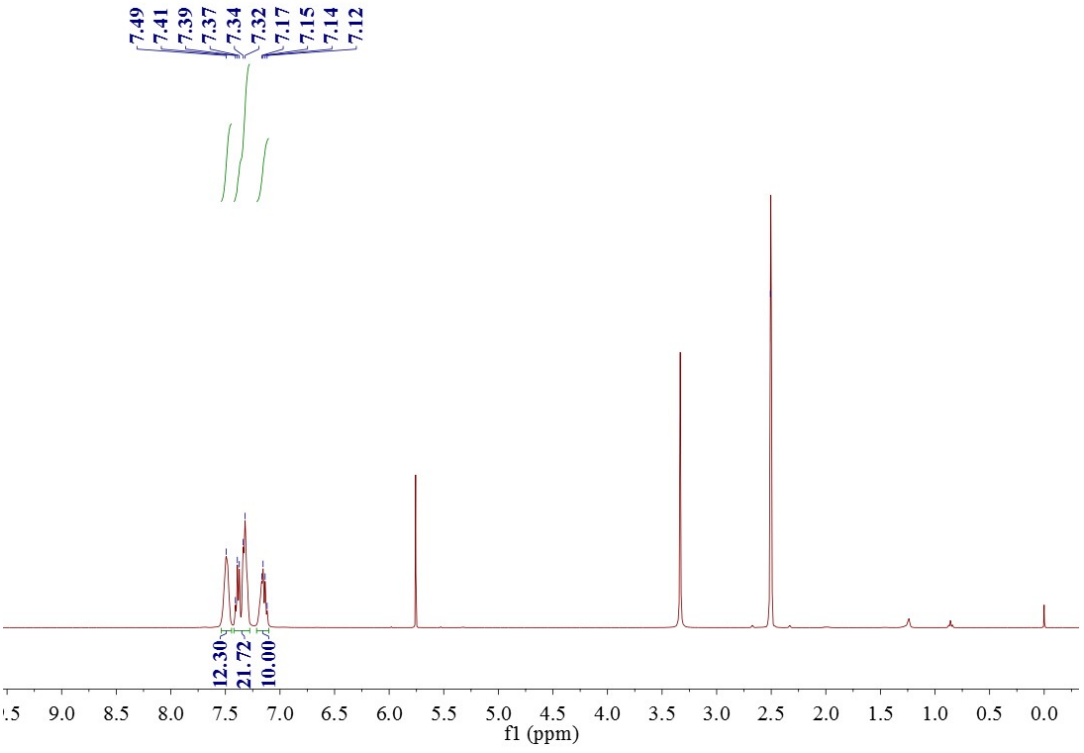


**Figure S8**. $^{1}H$ NMR spectrum of **3** in $d_6$-DMSO ($\delta$ = 5.76, $CH_2Cl_2$ residual peak).

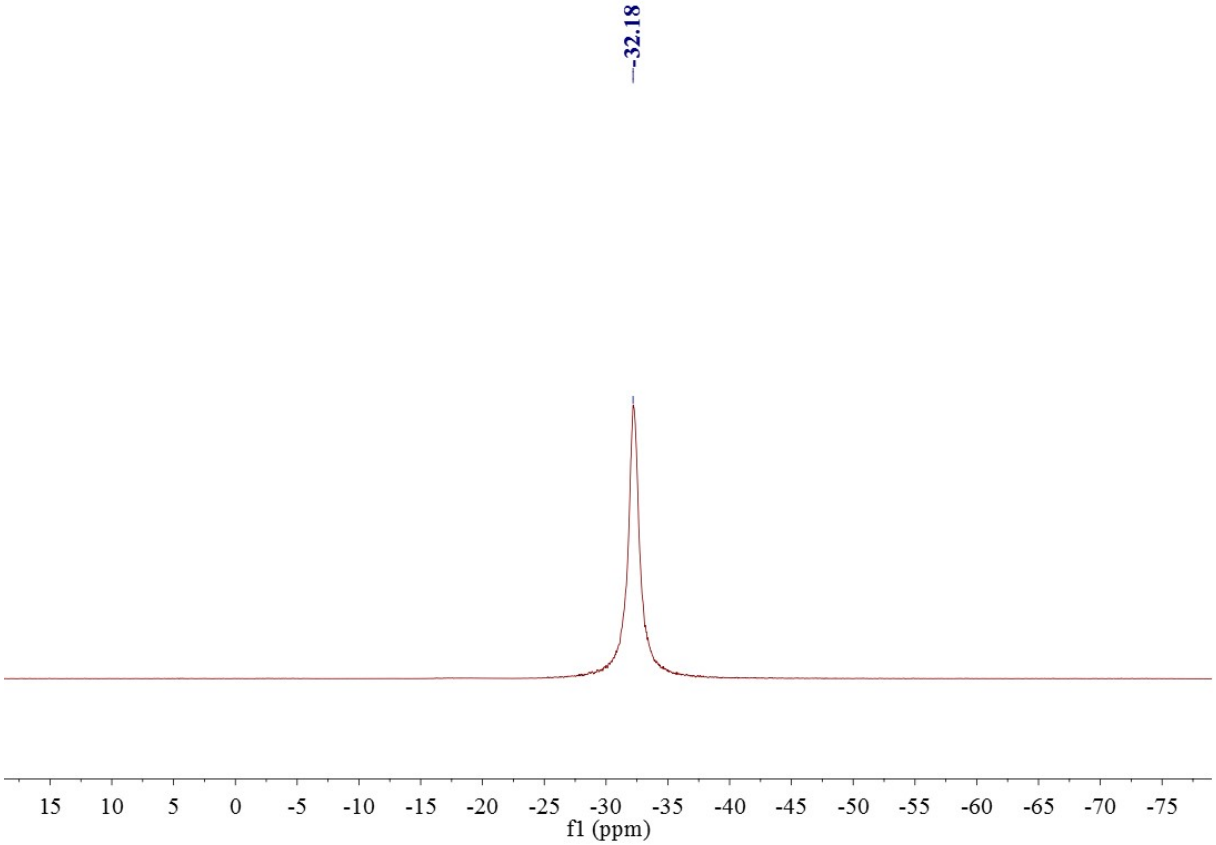


**Figure S9**. $^{31}P$ NMR spectrum of **3** in $CDCl_3$.

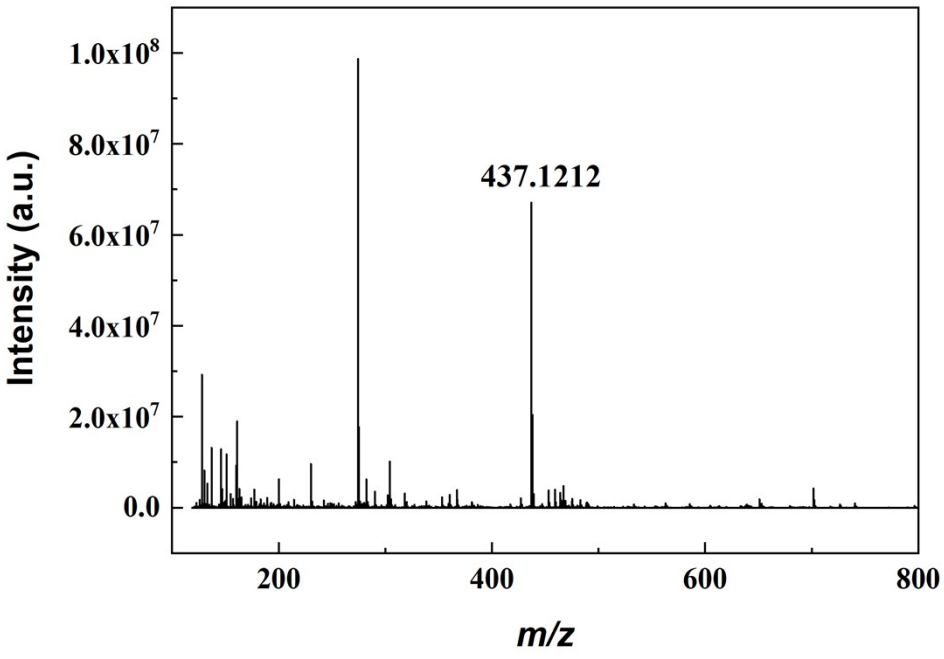


**Figure S10**. Mass spectrum of **dppf**.

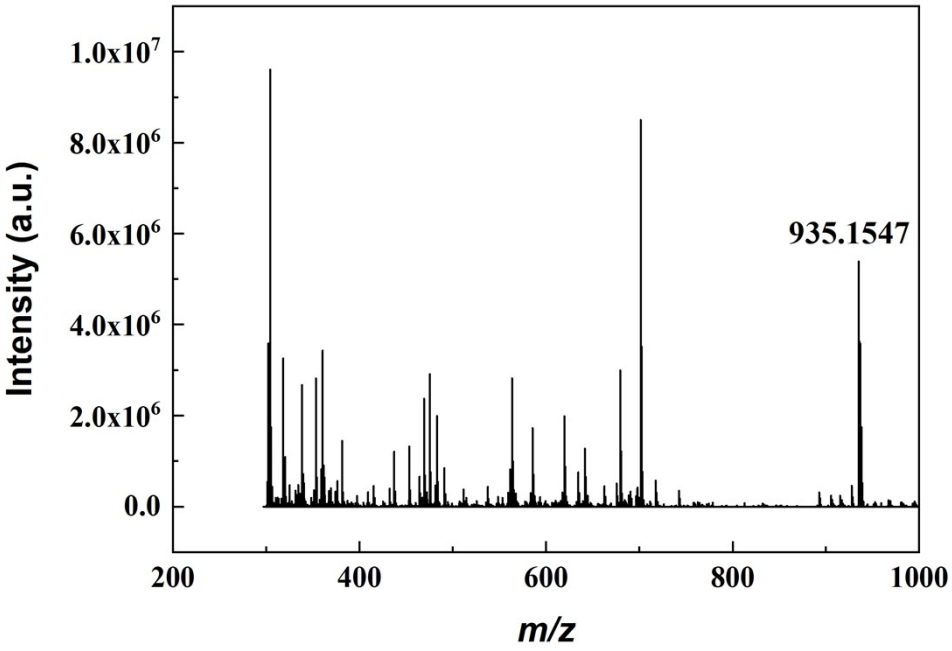


**Figure S11**. Mass spectrum of **1**.

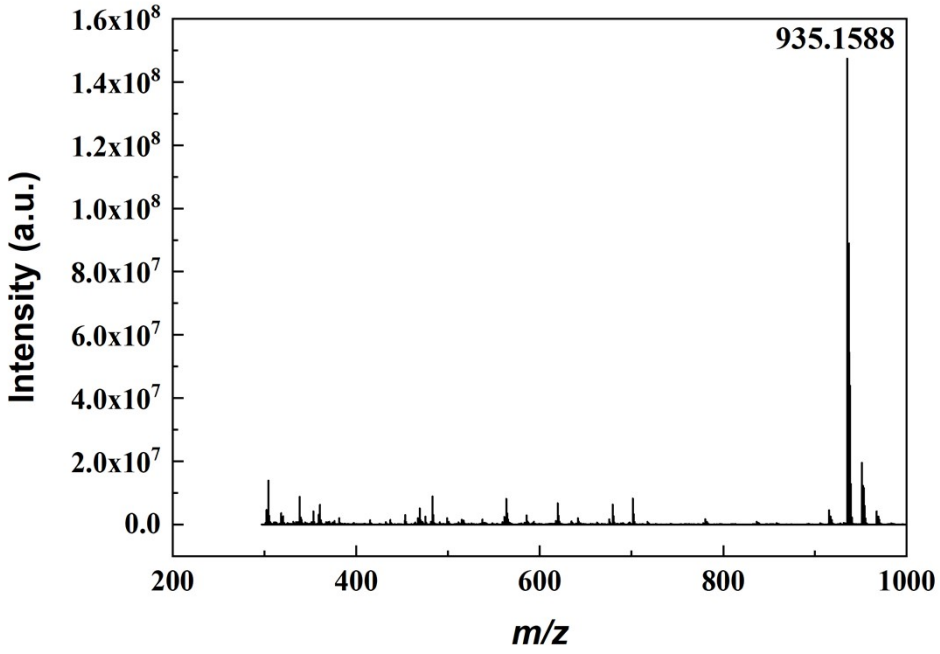


**Figure S12**. Mass spectrum of **2**.

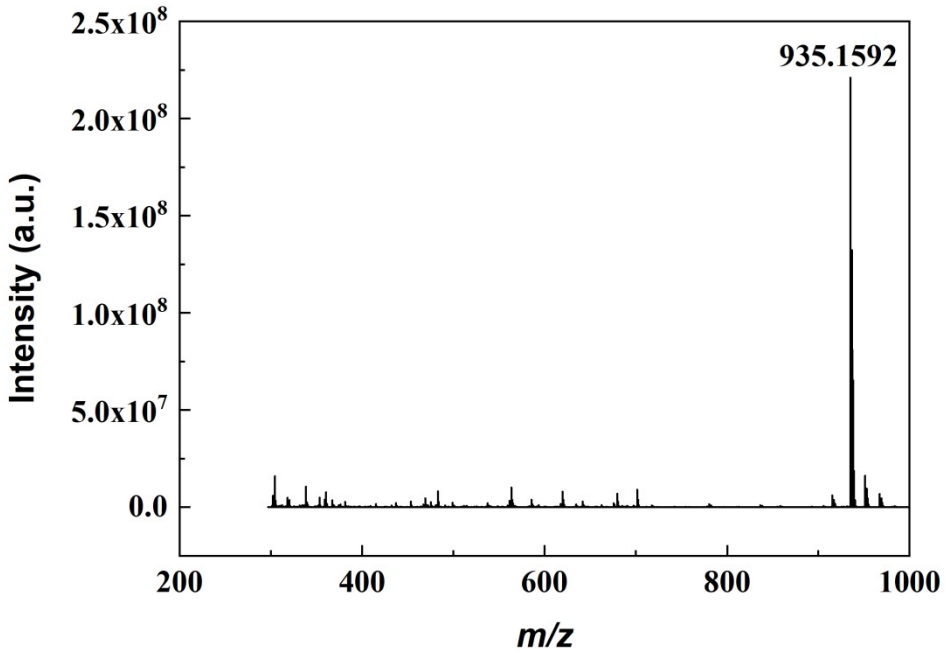


**Figure S13**. Mass spectrum of **3**.

## 3. Photophysical Properties

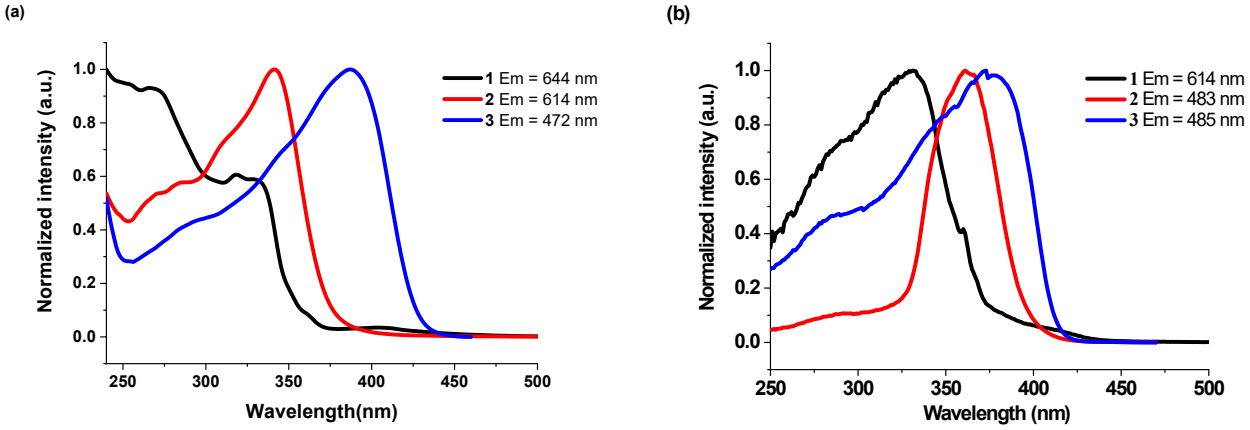


**Figure S14**. Normalized excitation spectra of complexes **1–3** in powder at 297 K and 77 K.

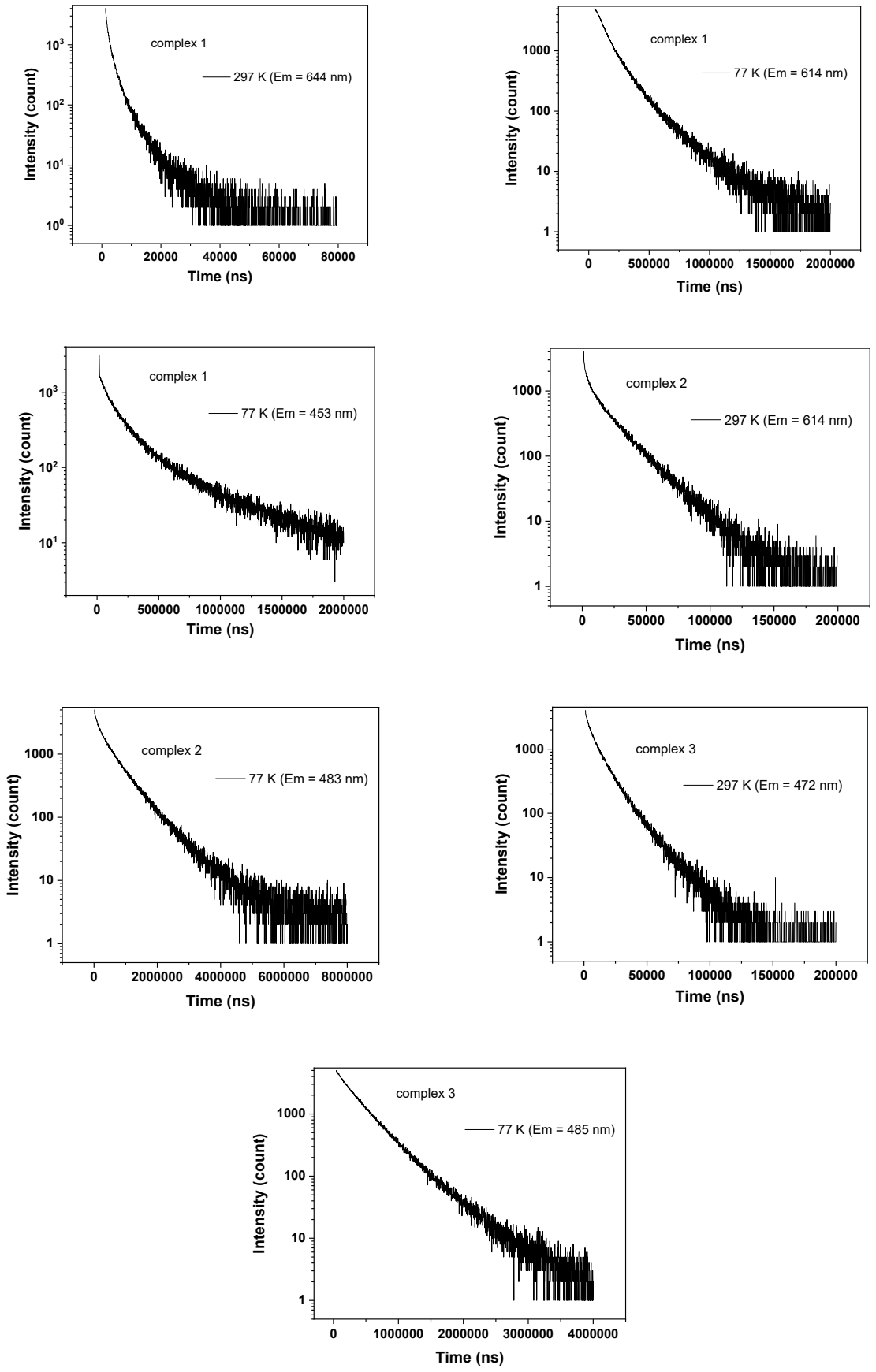


**Figure S15**. Time decay characteristics for complexes **1–3** in powder at 297 K and 77 K.

4. Theoretical calculation

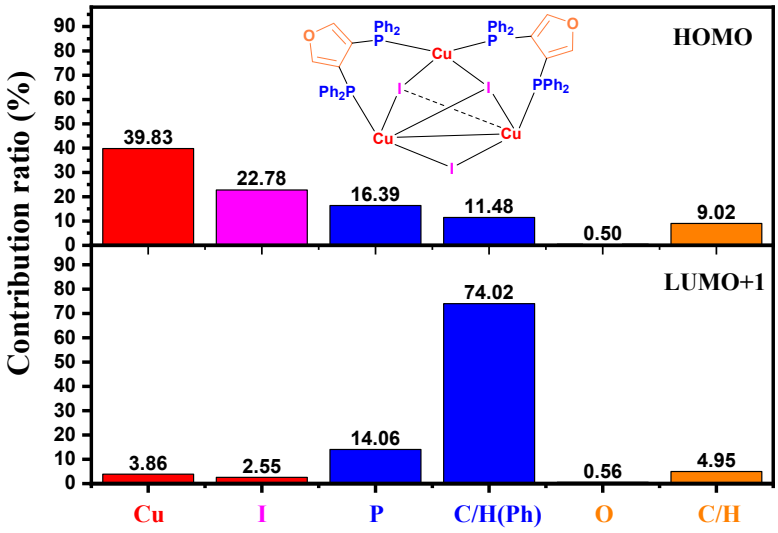


**Figure S16**. Compositions of the frontier molecular orbitals at optimized $S_0$ geometry of complex **1**.

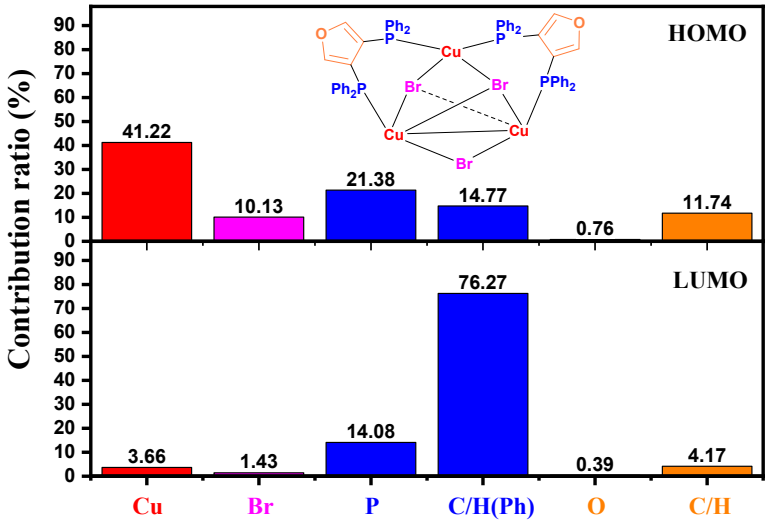


**Figure S17**. Compositions of the frontier molecular orbitals at optimized $S_0$ geometry of complex **2**.

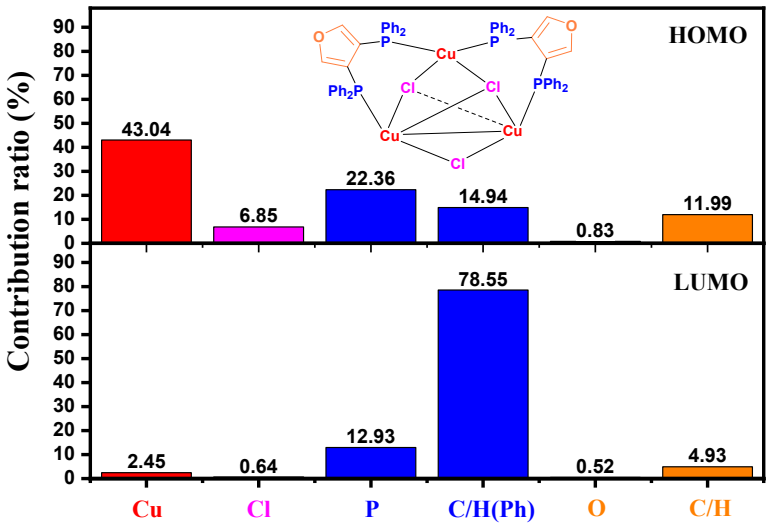


**Figure S18**. Compositions of the frontier molecular orbitals at optimized $S_0$ geometry of complex **3**.

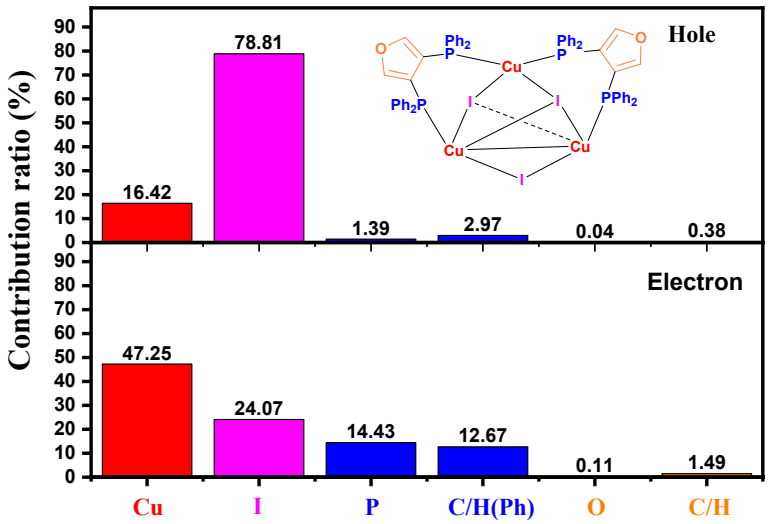


**Figure S19**. Compositions of the frontier molecular orbitals at optimized $T_1$ geometry of complex **1**.

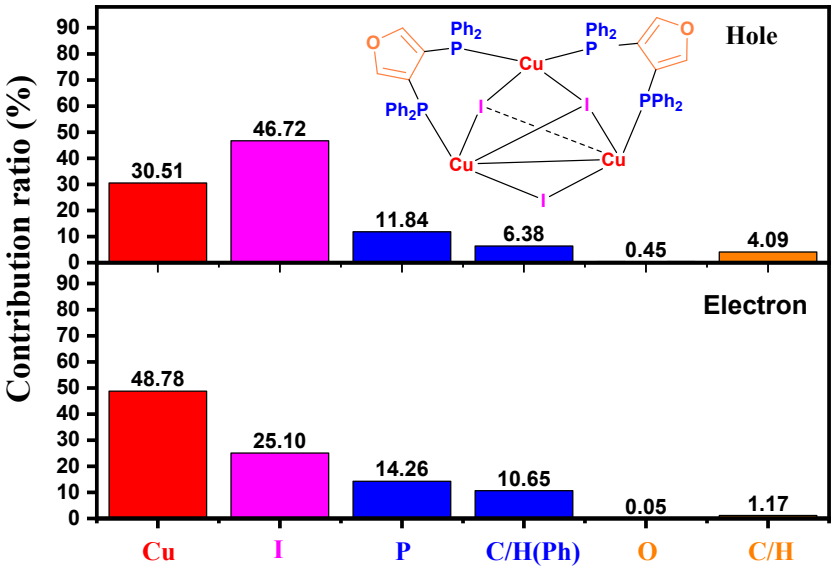


**Figure S20**. Compositions of the frontier molecular orbitals at optimized $T_2$ geometry of complex **1**.

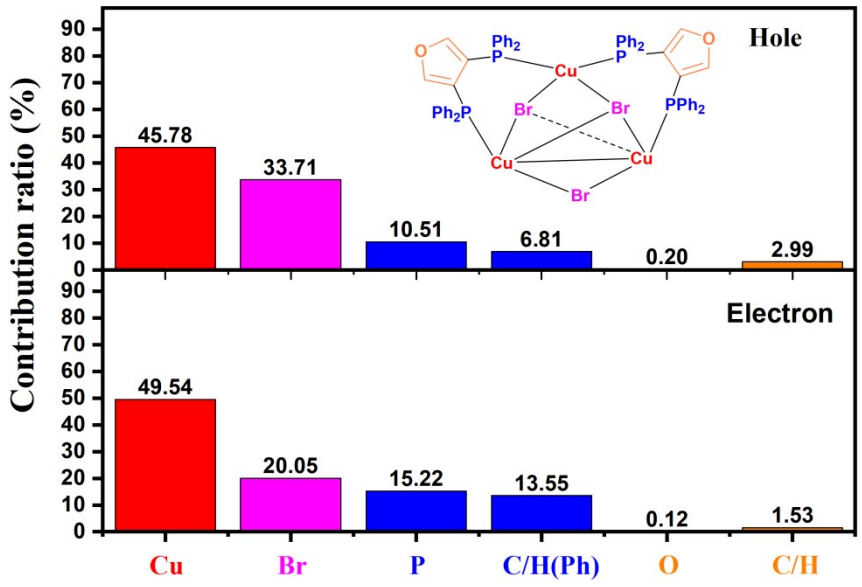


**Figure S21**. Compositions of the frontier molecular orbitals at optimized $T_1$ geometry of complex **2**.

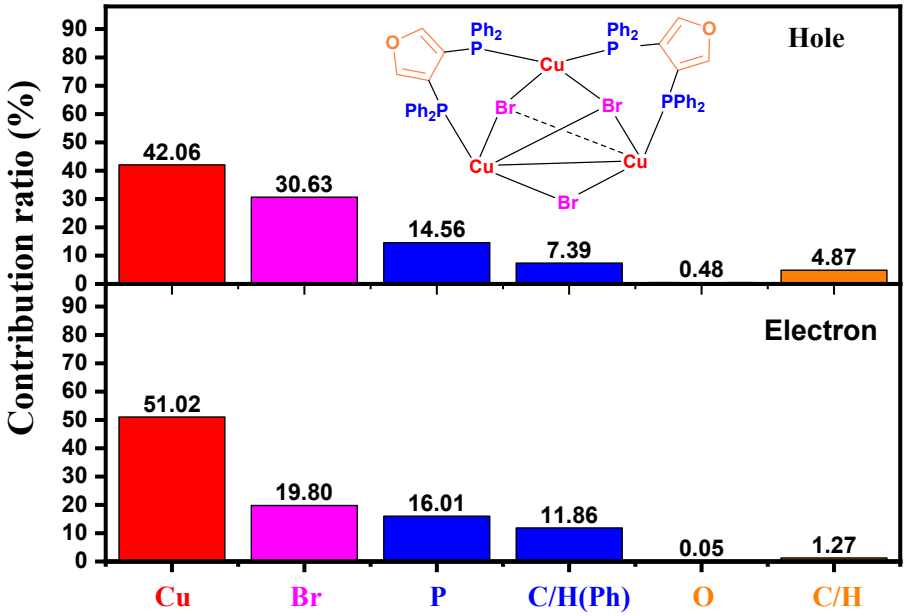


**Figure S22**. Compositions of the frontier molecular orbitals at optimized $T_2$ geometry of complex **2**.

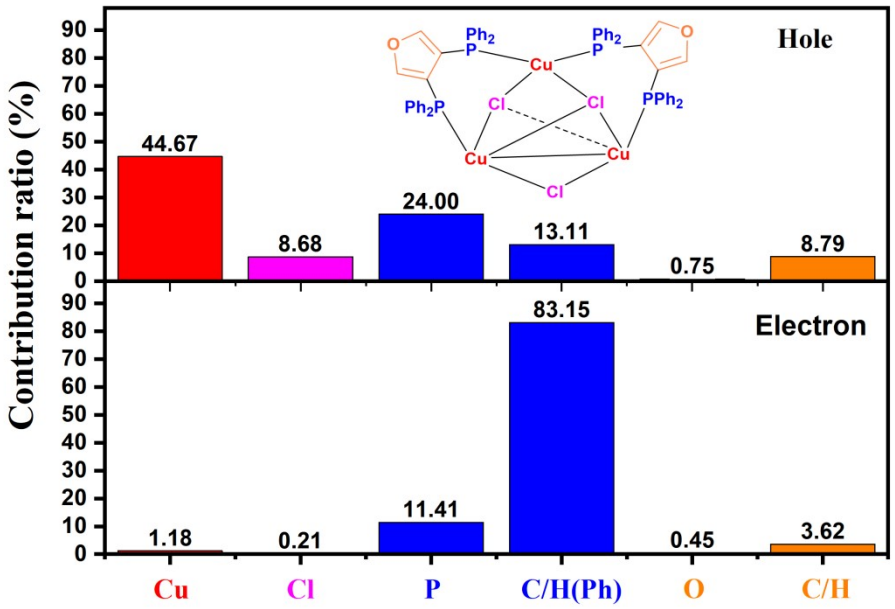


**Figure S23**. Compositions of the frontier molecular orbitals at optimized $S_1$ geometry of complex **3**.

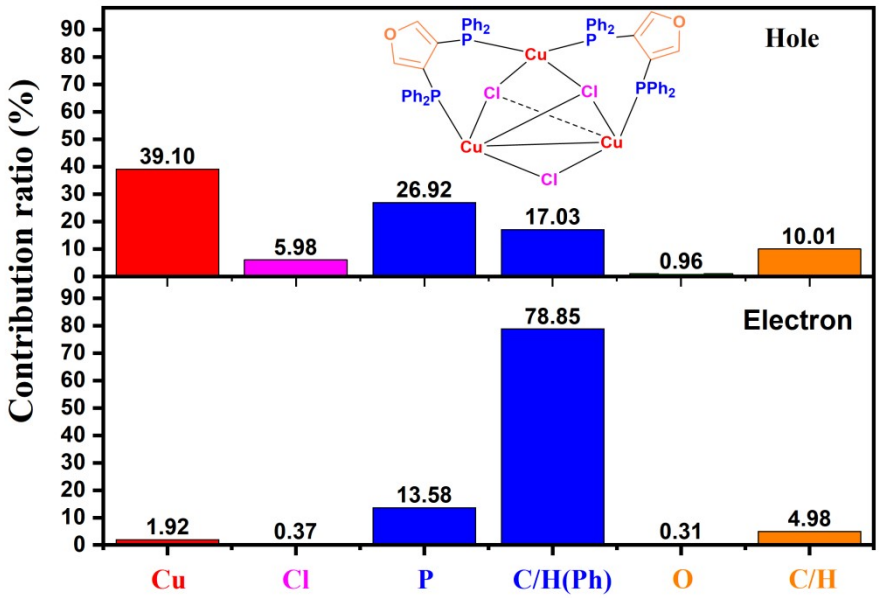


**Figure S24**. Compositions of the frontier molecular orbitals at optimized $T_1$ geometry of complex **3**.

**Table S1**. Crystallographic data and details for **1–3**.

| | **1** | **2** • $2(CH_2Cl_2)$ | **3** • $CH_2Cl_2$ |
|---|---|---|---|
| Empirical formula | $C_{56}H_{44}Cu_3I_3O_2P_4$ | $C_{56}H_{44}Cu_3Br_3O_2P_4$ • $2(CH_2Cl_2)$ | $C_{56}H_{44}Cu_3Cl_3O_2P_4$ • $CH_2Cl_2$ |
| Formula weight | 1444.11 | 1472.99 | 1254.69 |
| Temperature (K) | 297.06(10) K | 200.00(10) K | 199.99(10) K |
| Wavelength (Å) | 1.54184 | 1.54184 | 1.54184 |
| Crystal system | Orthorhombic | Monoclinic | Triclinic |
| Space group | Pbcn | $P2_1/n$ | P–1 |
| *a* (Å) | 18.0784(2) | 13.87931(5) | 12.78510(10) |
| *b* (Å) | 17.9614(2) | 25.12831(8) | 13.4486(2) |
| *c* (Å) | 18.4220(2) | 18.02014(7) | 18.4148(2) |
| *V* (Å$^3$) | 5981.87(11) | 5848.27(4) | 2809.91(6) |
| *Z* | 4 | 4 | 2 |
| $\rho$ (g cm$^{-3}$) | 1.604 | 1.673 | 1.483 |
| $\mu$(mm$^{-1}$) | 14.691 | 6.713 | 4.904 |
| *F* (0 0 0) | 2808 | 2928 | 1272 |
| $\theta$ range for data collection (°) | 5.984 to 67.476 | 3.168 to 74.107 | 3.550 to 74.529 |
| Index ranges | $21 \le h \le 21$<br>$21 \le k \le 21$<br>$16 \le l \le 22$ | $17 \le h \le 17$<br>$31 \le k \le 31$<br>$22 \le l \le 20$ | $15 \le h \le 15$<br>$16 \le k \le 16$<br>$22 \le l \le 22$ |
| Independent reflections | 5278 [R(int) = 0.0448] | 11744 [R(int) = 0.0281] | 10888 [R(int) = 0.0278] |
| Completeness to $\theta$ = 67.477° | 97.9 % | 99.5 % | 98.5 % |
| Max. and min. transmission | 1.00000 and 0.22040 | 1.00000 and 0.68336 | 1.00000 and 0.68148 |
| Gof | 1.045 | 1.048 | 1.050 |
| Final *R* indices [I > 2$\sigma$(*I*)] | $R_1$ = 0.0579<br>w$R_2$ = 0.1793 | $R_1$ = 0.0544<br>w$R_2$ = 0.1659 | $R_1$ = 0.0552<br>w$R_2$ = 0.1653 |
| *R* (all data) | $R_1$ = 0.0587<br>w$R_2$ = 0.1800 | $R_1$ = 0.0553<br>w$R_2$ = 0.1667 | $R_1$ = 0.0559<br>w$R_2$ = 0.1659 |
| Max/min (e Å$^3$) | 1.033 and –1.073 | 2.077 and –1.550 | 2.132 and –1.005 |

**Table S2**. Computed excitation transitions for complex **1** in $CH_2Cl_2$.

| State | λ(nm)/*E*(eV) | Configurations | *f* |
|---|---|---|---|
| 1 | 329.2 (3.77) | H→L+1 (87) | 0.0139 |
| 2 | 326.0 (3.80) | H-2→L (8); H-1→L+1 (11); H→L (76) | 0.0755 |
| 7 | 305.8 (4.06) | H→L+1 (5); H→L+3 (57); H→L+5 (11); H→L+6 (9); H→L+7 (4); H→L+9 (2); H→L+14 (3); H→L+17 (2) | 0.0349 |
| 9 | 300.6 (4.12) | H-4→L+1 (6); H-2→L (5); H-1→L+3 (29); H-1→L+5 (4); H→L+2 (28); H→L+4 (14) | 0.0459 |
| 32 | 279.1 (4.44) | H-4→L+3 (18); H-4→L+6 (5); H-3→L+4 (3); H-2→L+8 (44); H→L+10 (16) | 0.0437 |
| 45 | 272.2 (4.56) | H-7→L+1 (7); H-4→L+3 (15); H-4→L+5 (45); H-4→L+6 (4); H-4→L+7 (4); H-4→L+9 (2); H-1→L+9 (4) | 0.0351 |
| 56 | 267.4 (4.64) | H-7→L+1 (9); H-6→L (7); H-4→L+5 (3); H-4→L+7 (4); H-4→L+9 (6); H-2→L+12 (3); H-1→L+11 (10); H-1→L+14 (35); H→L+15 (2) | 0.0327 |
| 59 | 266.6 (4.65) | H-7→L (23); H-6→L+1 (18); H-1→L+12 (31); H-1→L+13 (6); H→L+14 (5) | 0.0322 |
| 84 | 255.3 (4.86) | H-7→L+2 (3); H-6→L+3 (8); H-5→L+2 (3); H-4→L+10 (33); H-3→L+11 (7); H-2→L+14 (3); H-2→L+17 (25); H-1→L+15 (3) | 0.0364 |

*f*: oscillator strength

**Table S3**. Computed excitation transitions for complex **2** in $CH_2Cl_2$.

| State | λ(nm)/*E*(eV) | Configurations | *f* |
|---|---|---|---|
| 1 | 329.8 (3.76) | H→L (74); H→L+1 (17) | 0.0296 |
| 2 | 325.8 (3.80) | H→L (17); H→L+1 (75) | 0.0689 |
| 8 | 302.4 (4.10) | H-3→L (2); H-2→L (27); H-2→L+1 (10); H-1→L (5); H→L+2 (5); H→L+3 (35); H→L+4 (4); H→L+5 (5) | 0.0451 |
| 13 | 290.5 (4.27) | H-3→L (3); H-2→L+2 (22); H-2→L+3 (7); H-2→L+4 (2); H-2→L+6 (2); H-1→L+1 (2); H-1→L+2 (7); H-1→L+3 (8); H-1→L+4 (28); H→L+6 (5) | 0.0303 |
| 14 | 288.7 (4.29) | H-3→L (22); H-3→L+1 (2); H-1→L+5 (4); H→L+4 (4); H→L+6 (37); H→L+8 (10) | 0.0311 |
| 25 | 279.1 (4.44) | H-4→L+1 (3); H-2→L+5 (12); H-2→L+6 (14); H-2→L+7 (2); H-1→L+6 (8); H→L+9 (44) | 0.0478 |
| 26 | 278.2 (4.46) | H-2→L+5 (12); H-1→L+6 (35); H-1→L+8 (6); H→L+9 (20); H→L+10 (2) | 0.0320 |
| 61 | 257.6 (4.81) | H-7→L (5); H-7→L+1 (4); H-6→L+1 (18); H-5→L+4 (2); H-4→L+5 (7); H-3→L+6 (4); H-2→L+10 (8); H-2→L+12 (2); H-1→L+14 (3); H→L+15 (3); H→L+16 (16) | 0.0361 |
| 80 | 251.2 (4.94) | H-11→L (3); H-9→L (3); H-9→L+1 (6); H-8→L (8); H-8→L+1 (4); H-6→L+2 (2); H-4→L+7 (25); H-2→L+10 (2); H-2→L+17 (4); H-1→L+14 (3); H→L+18 (3) | 0.0354 |
| 92 | 246.7 (5.03) | H-14→L (3); H-13→L (6); H-12→L (7); H-11→L (4); H-10→L (2); H-10→L+1 (2); H-6→L+5 (4); H-5→L+7 (6); H-5→L+8 (3); H-4→L+8 (2); H-4→L+9 (4); H-3→L+9 (3); H-2→L+15 (4); H-2→L+16 (4); H-1→L+15 (4); H→L+19 (6) | 0.0316 |

**Table S4**. Computed excitation transitions for complex **3** in $CH_2Cl_2$.

| State | λ(nm)/*E*(eV) | Configurations | *f* |
|---|---|---|---|
| 1 | 332.0 (3.73) | H→L (69); H→L+1 (24) | 0.0324 |
| 2 | 329.2 (3.77) | H→L (25); H→L+1 (69) | 0.0648 |
| 11 | 291.7 (4.25) | H-3→L+1 (7); H-2→L+2 (19); H-1→L+2 (16); H-1→L+3 (2); H-1→L+4 (7); H→L+6 (29); H→L+7 (8) | 0.0318 |
| 14 | 287.6 (4.31) | H-3→L (3); H-3→L+1 (31); H-2→L+2 (2); H-2→L+3 (3); H-1→L+4 (4); H-1→L+5 (3); H→L+6 (14); H→L+8 (21) | 0.0417 |
| 21 | 280.3 (4.42) | H-3→L (4); H-2→L+2 (4); H-2→L+4 (3); H-2→L+6 (3); H-1→L+5 (5); H-1→L+6 (4); H→L+9 (52); H→L+10 (3); H→L+11 (3) | 0.0714 |
| 89 | 245.5 (5.05) | H-12→L+1 (3); H-10→L+1 (4); H-9→L (2); H-9→L+1 (3); H-7→L+2 (2); H-6→L+2 (29); H-6→L+5 (2); H-4→L+8 (2); H-2→L+15 (3); H-1→L+16 (4); H-1→L+18 (3) | 0.0367 |

## 5. Thermal properties

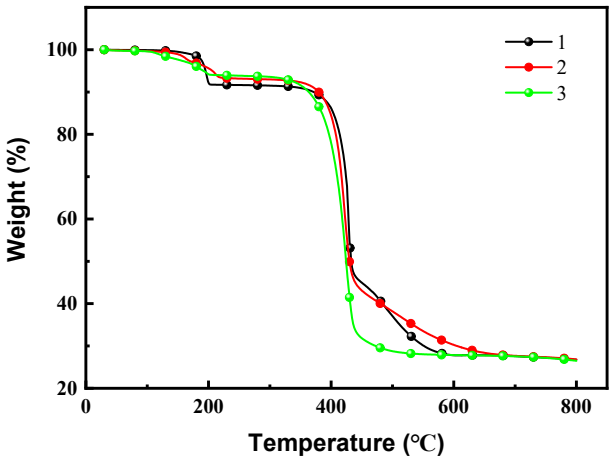


**Figure S25**. TGA curves of complexes **1–3**.

The thermal properties of complexes **1–3** in powder state are studied by thermogravimetric analysis (TGA) under a stream of nitrogen. From the onset of the TGA curves (Figure S25), complexes **2** and **3** show good thermal stability with their $T_{dec}$ values of 397 °C and 425 °C, respectively, the small weight loss of ca. ~ 6% below 202 °C for **2** and

221 °C for **3** is ascribed to the removal of solvent molecules. Complex **1** showed the weight loss of ca. 8.2% at 202 °C, corresponding to the removal of one halogen I atom. Large weight loss of ca. 72% were observed between 397 °C and 665 °C for complexes **1–3**, which is due to the removal of halogen left and decomposition of ligand **dppf**.

## 6. References


(1) G. A. Kraus and X. Wang, An Improved Synthesis of 3-Substituted Furans from Substituted Butene-1,4-diols, *Synthetic Commun.*, 1998, **28**, 1093−1096.

(2) *SAINT Reference Manual*, Siemens Energy and Automation, Madison, WI, 1994.

(3) G. M. Sheldrick, *SADABS*, *Empirical Absorption Correction Program*, University of Göttingen, Göttingen, Germany, 1997.

(4) G. M. Sheldrick, *SHELXTL Reference Manual*, *Version 5.1*, Siemens Energy and Automation, Madison, WI, 1997.

(5) M. J. Frisch, G. W. Trucks, H. B. Schlegel, G. E. Scuseria, M. A. Robb, J. R. Cheeseman, G. Scalmani, V. Barone, G. A. Petersson, H. Nakatsuji, X. Li, M. Caricato, A. V. Marenich, J. Bloino, B. G. Janesko, R. Gomperts, B. Mennucci, H. P. Hratchian, J. V. Ortiz, A. F. Izmaylov, J. L. Sonnenberg, D. Williams-Young, F. Ding, F. Lipparini, F. Egidi, J. Goings, B. Peng, A. Petrone, T. Henderson, D. Ranasinghe, V. G. Zakrzewski, J. Gao, N. Rega, G. Zheng, W. Liang, M. Hada, M. Ehara, K. Toyota, R. Fukuda, J. Hasegawa, M. Ishida, T. Nakajima, Y. Honda, O. Kitao, H. Nakai, T. Vreven, K. Throssell, J. A. Montgomery, Jr., J. E. Peralta, F. Ogliaro, M. J. Bearpark, J. J. Heyd, E. N. Brothers, K. N. Kudin, V. N. Staroverov, T. A. Keith, R. Kobayashi, J. Normand, K. Raghavachari, A. P. Rendell, J. C. Burant, S. S. Iyengar, J. Tomasi, M. Cossi, J. M. Millam, M. Klene, C. Adamo, R. Cammi, J. W. Ochterski, R. L. Martin, K. Morokuma, O. Farkas, J. B. Foresman, and D. J. Fox, Gaussian 16, Revision A.03, Gaussian Inc., Wallingford CT, 2016.

(6) T. Lu and F. W. Chen, Calculation of Molecular Orbital Composition, *Acta Chim. Sinica* 2011, **69**, 2393−2406.

(7) T. Lu and F. W. Chen, Multiwfn: a multifunctional wavefunction analyzer, *J. Comput. Chem.* 2012, **33**, 580−592.